Phase Transitions under Strong Magnetic Fields in Neutron Star

Ishfaq A. Rather[1,*], *Veronica* Dexheimer[2,**], and *Ilídio* Lopes[1,***]

[1]Centro de Astrofísica e Gravitação-CENTRA, Instituto Superior Técnico-IST, Universidade de Lisboa-UL, Av. Rovisco Pais, 1049-001 Lisboa, Portugal
[2]Department of Physics, Kent State University, Kent OH 44242 USA

Abstract. A comprehensive study is carried out on the impact of strong magnetic fields on the deconfinement phase transition inside massive neutron stars. The matter equation of state and the general relativity solutions, which also fulfill Maxwell's equations, are modified when taking magnetic-field effects into account. We observe that the maximum mass and canonical-mass radius of stars computed using spherically-symmetric TOV equations and axisymmetric solutions obtained through the LORENE library differ significantly for large values of magnetic dipole moment. The discrepancies depend on the stellar mass being studied, as well as the stiffness of the equation of state. This indicates that the matter composition and interactions determine the magnetic field thresholds for the acceptable approximation of isotropic stars and the appropriate application of TOV equations.

1 Introduction

One of the most prominent and intriguing areas of research at the moment is the behavior of matter under extreme densities, temperatures, and magnetic fields. For studying physics in extreme conditions, neutron stars (NSs) are the ideal environment. Intriguing conclusions about NSs maximum mass, canonical mass, radius, tidal deformability, and other characteristics have been drawn as a result of recent advancements in observation. The equation of state (EoS) of the dense matter is, nevertheless, still widespread with uncertainty. Given that the density inside NSs is several times that of nuclear saturation ($\rho_0 \approx 10^{14}$ g cm^{-3}), it is challenging to ascertain their internal structure. Theoretical models describing cold and dense matter, calibrated around ρ_0 for isospin-symmetric nuclear matter (SNM), must be extrapolated in both density and isospin asymmetry as stellar inner densities approach 10^{15} g cm^{-3}. The structure of NSs is computed starting with the energy-momentum tensor, solving equations for hydrostatic equilibrium, and comparing them to astrophysical observations in order to evaluate these theories. The ability to explain the maximum measured NS mass, which according to the latest astrophysical data is above $2M_\odot$, is one criterion that all NS models must achieve [1, 2].

NSs have been known to possess immensely strong magnetic fields in addition to being extremely dense objects. Surface magnetic fields of $\sim 10^{12}$–10^{13} G are already generated by combining a straightforward magnetic dipole model with known pulsar spin-down data [3]. The virial theorem is widely used to estimate the maximum magnetic field in the core of magnetars because it is not possible to measure it directly. According to most estimations, the field will have a theoretical maximum of 10^{18} G [4]. Strong magnetic fields can affect NSs in a number of ways, including changing the energy-momentum tensor, changing the EoS due to Landau quantization of the constituent charged particles, and breaking stellar spherical symmetry. It should be emphasized that the deviations from spherical symmetry for intense magnetic fields, however, can already be significantly below the threshold at which Landau quantization effects on the EoS become non-negligible [5]. In this case, Spherically symmetric TOV equations can no longer be used to describe the macroscopic structure of NS configurations. In the following, we discuss what this limit is in terms of the magnetic field strength and EoS.

2 Formalism

2.1 Nuclear Matter

For the description of hadronic matter, the DD-RMF model is used with the Lagrangian density given by

$$\begin{aligned}\mathcal{L}_m = &\sum_b \bar{\psi}_b \Big\{ \gamma_\mu \Big(i D^\mu - g_\omega(\rho_b)\omega_\mu - \frac{1}{2} g_\rho(\rho_b)\rho_\mu \tau \Big) \\ &- \Big(M_b - g_\sigma(\rho_b)\sigma \Big) \Big\} \psi_b + \frac{1}{2} \Big(\partial^\mu \sigma \partial_\mu \sigma - m_\sigma^2 \sigma^2 \Big) \\ &- \frac{1}{4} W^{\mu\nu} W_{\mu\nu} + \frac{1}{2} m_\omega^2 \omega_\mu \omega^\mu - \frac{1}{4} R^{\mu\nu} R_{\mu\nu} + \frac{1}{2} m_\rho^2 \rho_\mu \rho^\mu \\ &+ \sum_l \bar{\psi}_l (i\gamma_\mu D^\mu - m_l) \psi_l \,, \end{aligned} \tag{1}$$

where b sums over the baryon octet and l over non-interacting leptons. ψ_b and ψ_l represent the baryon and lepton Dirac fields and M_b and m_l the baryon and lepton masses, respectively. The density-dependent coupling

*e-mail: ishfaq.rather@tecnico.ulisboa.pt
**e-mail: vdexheim@kent.edu
***e-mail: ilidio.lopes@tecnico.ulisboa.pt

constants for the DD-RMF parameter set are written as a function of baryon density ρ_B

$$g_i(\rho_B) = g_i(\rho_0) f_i(x) \,, \tag{2}$$

where the function $f_i(x)$ is given by

$$f_i(x) = a_i \frac{1 + b_i(x + d_i)^2}{1 + c_i(x + d_i)^2}, \; i = \sigma, \omega \,. \tag{3}$$

The coupling of the hyperons to the σ meson coupling constants is determined at saturation from fitting the Λ hyperon optical potential for SNM to results obtained from lattice calculations [6], reproducing the well-known potentials.

2.2 Quark Matter

The vector-enhanced bag (vBag) model is used to describe the quark matter while allowing hybrid stars to fulfill the $2M_\odot$ maximum mass limit [8–10].

The Lagrangian density for the vBag model is given by [7]

$$\begin{aligned}\mathcal{L} = & \sum_{f=u,d,s} [\psi_f(i\gamma_\mu \partial_\mu - m_f - B)\psi_f]\Theta_H \\ & - G_V \sum_f (\bar{\psi_f}\gamma_\mu \psi_f)^2 + \sum_l \psi_l \gamma_\mu (i\partial_\mu - m_l)\psi_l \,, \end{aligned} \tag{4}$$

where B denotes the bag constant and Θ_H is the Heaviside step function that allows for a confinement/deconfinement of the bag [11]. The vector interaction is introduced via the coupling of vector-isoscalar meson to the quarks with coupling constant G_V.

The expressions for the energy density and pressure for a single quark flavor are defined as

$$\mathcal{E}_{\text{vBag,f}} = \mathcal{E}_f(\mu_f^*) + \frac{1}{2} K_\nu n_f^2(\mu_f^*) + B_{\chi,f} \,, \tag{5}$$

$$P_{\text{vBag,f}} = P_f(\mu_f^*) + \frac{1}{2} K_\nu n_f^2(\mu_f^*) - B_{\chi,f} \,. \tag{6}$$

Here $B_{\chi,f}$ is the bag constant for a single quark flavor. The vector interaction parameter K_ν controls the stiffness of matter [12].

2.3 Mixed Phase

Charge neutrality is achieved globally using a Gibbs construction [13]. The extension of the mixed phase in density depends on the stiffness of the phases undergoing chemical equilibrium. Within the mixed-phase region, the expressions for the chemical potential and pressure are defined as

$$\mu_{B,H} = \mu_{B,Q}; \;\; \mu_{e,H} = \mu_{e,Q} \,, \tag{7}$$

and

$$P_H(\mu_B, \mu_e) = P_Q(\mu_B, \mu_e) = P_{MP} \,, \tag{8}$$

with the subscripts H, Q, and MP representing the hadronic phase, quark phase, and mixed-phase, respectively.

3 Magnetic Field

To investigate the effects of magnetic fields on our microscopic description of matter with a phase transition, we use a chemical-potential dependent magnetic field that is fitted from the solutions of the Einstein-Maxwell equations. The magnetic field-chemical potential relationship is dependent on the magnetic dipole moment and is provided by the relation [14]

$$B^*(\mu_B) = \frac{(a + b\mu_B + c\mu_B^2)}{B_c^2} \mu \,, \tag{9}$$

where μ_B is the baryon chemical potential in MeV and μ is the dipole magnetic moment in units of Am^2, so as to produce B^* in units of the electron critical field $B_c = 4.414 \times 10^{13}$ G. The coefficients a, b, and c taken as $a = -0.786$ G^2/(Am^2), $b = 1.24 \times 10^{-3}$ G^2/(Am^2 MeV) and $c = -3.51 \times 10^{-7}$ G^2/(Am^2 MeV^2) are obtained from a fit for the magnetic field in the polar direction of a star with a baryon mass of 2.2 M$_\odot$.

For the effective bag constant $B_{\text{eff}}^{1/4} = 130$ and 150 MeV, the magnetic field at the stellar center is 3×10^{17} G and 1×10^{18} G, respectively for $\mu = 5 \times 10^{31}$ Am^2. With $\mu = 2{\times}10^{32}$ Am^2, the magnetic field goes upto $3.2{\times}10^{17}$ G and $1.2{\times}10^{18}$ G for $B_{\text{eff}}^{1/4} = 130$ and 150 MeV, respectively.

The expressions for the free quark matter energy density and pressure in the presence of the magnetic field are shown in [15]. In presence of the magnetic field, the total energy density is

$$\mathcal{E} = \mathcal{E}_m + \frac{B^2}{8\pi} \,, \tag{10}$$

and the total pressure in transverse and polar directions to the local magnetic field is

$$P_\perp = P_m - \mathcal{M}B + \frac{B^2}{8\pi}, \;\; P_\parallel = P_m - \frac{B^2}{8\pi} \,, \tag{11}$$

where the magnetization is calculated as

$$\mathcal{M} = \partial P_m / \partial B \,. \tag{12}$$

To ascertain the stellar properties of magnetic NSs, we employ the LORENE library [16, 17], which solves the Einstein-field Maxwell's equations with an axisymmetric deformation. When instead pressure in the local perpendicular direction to the magnetic field is applied in all directions, the spherically symmetric solutions obtained by solving the TOV equations lead to an overestimation of the mass and an underestimation of the equatorial radius and therefore cannot be used to determine stellar properties [5, 16]. In this work, we use both approaches for comparison.

4 Results and Discussion

To study the effect of a strong magnetic field on the hadron-quark phase transition, we employed the DD-MEX parameter set for the hadronic matter as it produces a very stiff EoS. For quark matter, two values of the effective bag

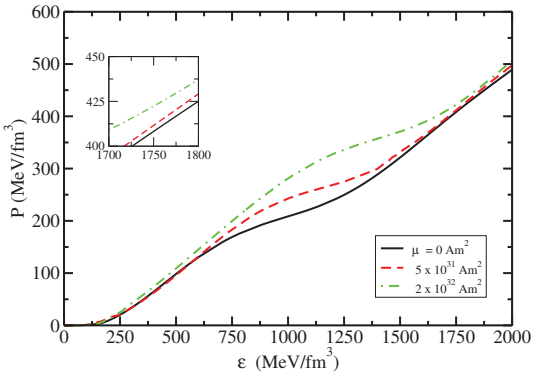

Figure 1. Energy density vs. transverse pressure at different values of dipole magnetic moment for the EoS with effective bag constant $B_{\rm eff}^{1/4}$ = 130 MeV.

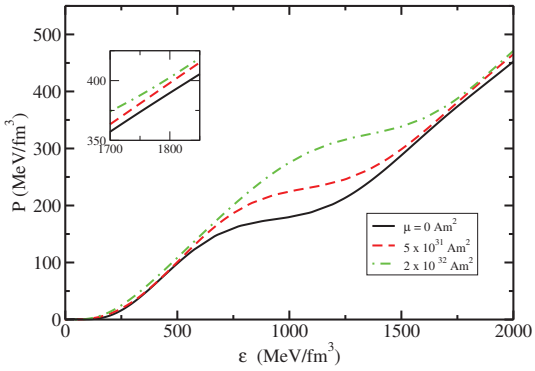

Figure 2. Same as Fig. 1, but for $B_{\rm eff}^{1/4}$ = 150 MeV.

constant, $B_{\rm eff}^{1/4}$ = 130 and 150 MeV are used, and the coupling constant parameter K_ν is fixed at 4 GeV^{-2}.

Fig. 1 displays the NS EoS with quark deconfinement with effective bag constant $B_{\rm eff}^{1/4}$ = 130 MeV in the presence of the magnetic field profile for different values of the magnetic dipole moment. For the lower effective bag constant, the hadronic phase in the low-density region is largely unchanged by the magnetic field, whereas the pure quark phase in the high density is slightly stiffer than the EoS without the magnetic field for the magnetic dipole moment of $\mu = 5 \times 10^{31}$ Am^2, which corresponds to a high-density magnetic field of $\sim 10^{17}$ G. Both the hadronic phase and the pure quark phases stiffen up for the magnetic dipole moment of $\mu = 2 \times 10^{32}$ Am^2, which is equivalent to a $\sim 10^{18}$ G high-density magnetic field.

Fig. 2 displays the EoS for effective bag constant $B_{\rm eff}^{1/4}$ = 150 MeV. The pure quark phase only comprises a minimal portion (if any) of NSs since it only appears at very high densities. The beginning of the mixed phase and the pure quark phase are both significantly impacted by the increased effective bag constant. This is because the magnetic field is significantly greater at the densities where it occurs. Consequently, it is clear that the inclusion of the magnetic field and its strength have an impact on the transitions to the mixed phase and the pure quark phase. The magnetic field also suppresses the hyperons that emerge around the onset of mixed-phase due to an increased proton density.

The mass-radius diagram for hybrid stars computed for effective bag constant $B_{\rm eff}^{1/4}$ = 130 MeV without and with magnetic field estimated for various values of the magnetic dipole moment is shown in Fig. 3. The left panel displays the results obtained from solving Einstein and Maxwell's equations with an axisymmetric deformation (LORENE library), and the right panel displays the results using answers from spherically symmetric TOV equations. For $\mu = B = 0$, they are exactly equivalent, which should be the case. The maximum mass star has a radius of 12.6 km is $2.13 M_\odot$ without a magnetic field. The canonical mass has a radius of about 13 km, which satisfies the recent NICER radius constraints. With increasing magnetic dipole moment, the mass and radius of entire stellar sequences increase. For $\mu = 5 \times 10^{31}$ Am^2, which corresponds to a magnetic field of 3×10^{17} G in the center of the maximum-mass star, the radius of low/intermediate-mass stars obtained using the LORENE library differs significantly from the radius obtained from TOV, 0.6 km for the canonical mass when compared with 0.1 km for the maximum mass. In the left panel of Fig. 3, the radius shown is the equatorial radius, and under the influence of strong poloidal magnetic fields, stars become oblate.

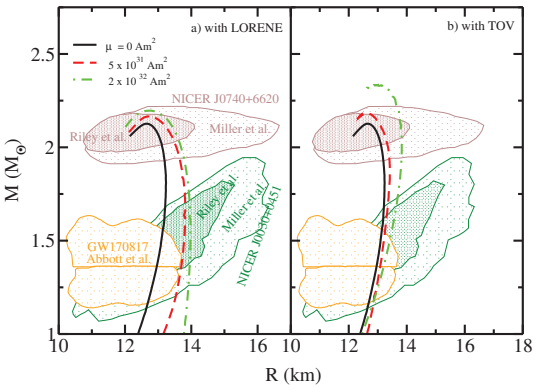

Figure 3. Mass-radius profile for hybrid stars with effective bag constant $B_{\rm eff}^{1/4}$ = 130 MeV shown at different values of magnetic dipole moment. The left panel shows results obtained using the LORENE library, while the right panel shows solutions from TOV. Recent constraints on mass and radius are also shown [1, 18–23].

Fig. 4 also displays the mass-radius profiles for hybrid stars but with effective bag constant $B_{\rm eff}^{1/4}$ = 150 MeV. For $\mu = 0$, the maximum mass obtained lowers to 2.08 $M_\odot$ with corresponding radius of 12.76 km. The radius at the canonical mass is 12.85 km. Our results are still in agreement with NICER, LIGO/VIRGO, and mass constraints. Using LORENE, as the magnetic dipole moment increases, the maximum mass increases more than for the previous effective bag constant considered. The radius of the whole sequence also increases more. The solutions from TOV, do not depend as much on the effective bag constant, and in this case, are farther from reproducing low/intermediate mass results from LORENE. A difference of around 0.5 km is observed in the radius at

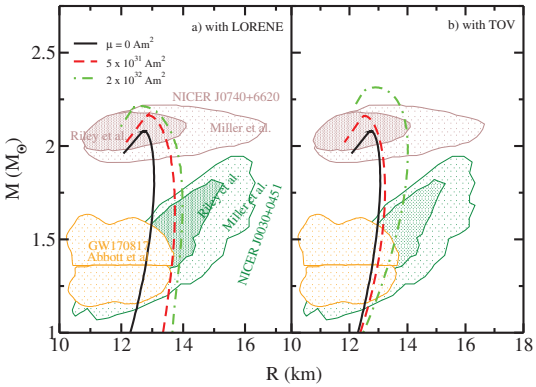

Figure 4. Same as Fig. 3, but for $B_{\rm eff}^{1/4} = 150$ MeV.

the canonical mass and −0.3 for the maximum mass with measurements from LORENE and TOV. This implies that the difference between the two approaches depends on the EoS (particle composition and interactions) and the mass of the star we are calculating the deformation for.

Considering the rotation along with the magnetic field, the ratio between the polar and the equatorial radii would increase and the resulting star would be deformed more. The difference between these two radii would depend on the star's rotation rate, the strength of the magnetic field, and the properties of the stellar matter.

5 Summary and Conclusion

We investigated how strong magnetic fields influence the transition from baryons to quarks in NS cores. A magnetic field profile with a quadratic relationship with the chemical potential is used to investigate the effects of magnetic fields on the EoS. In this setup, the magnetic field only really depends on the magnetic dipole moment at high densities, reaching 10^{18} G for the largest magnetic dipole moment studied. Magnetic fields cause the EoS to stiffen, although the effects are more pronounced in the mixed phase, which is wider in terms of energy density and occurs at higher densities. Larger magnetic dipole moments and effective bag constants have stronger impacts.

The poloidal magnetic field makes NSs oblate using the LORENE library, enlarging the equatorial radius. While the magnetic field affects the mass and radius of all stars in a family, this is not the case for TOV, which results in the rise of only massive stars and an unreasonably huge increase in their masses. The effective bag constant has no bearing on this qualitative behavior. The mass and radii of the entire family of stars defined by a lower effective bag constant (softer EoS) utilizing LORENE are quantitatively impacted by the strong magnetic field.

The difference in radius between LORENE and TOV for particular constant stellar masses is interestingly higher with lower values of μ and B. The canonical radius is consistently smaller for TOV overall, and the disparity grows with the effective bag constant. TOV can have a smaller or larger radius than LORENE for the radius of the maximum-mass star, depending upon whether the μ is small or large. The sequence's maximum mass is always too large for TOV, and this disparity gets more as μ and the effective bag constant increases.

Acknowledgement

I. A. R. and I. L. acknowledge the Fundação para a Ciência e Tecnologia (FCT), Portugal, for the financial support to the Center for Astrophysics and Gravitation (CENTRA/IST/ULisboa) through the grant Project No. UIDB/00099/2020 and grant No. PTDC/FIS-AST/28920/2017. V. D. acknowledges support from the National Science Foundation under grants PHY1748621, MUSES OAC-2103680, and NP3M PHY-2116686.

References

[1] J. Antoniadis, P.C.C. Freire *et al.*, Science **340** (2013)
[2] E. Fonseca et al., Astrophys. Jour. L. **915**, L12 (2021)
[3] S.B. Popov, R. Turolla, A. Possenti, MNRAS **369**, L23 (2006)
[4] D. Lai, S.L. Shapiro, Astrophys. Jour. **383**, 745 (1991)
[5] R.O. Gomes, H. Pais, V. Dexheimer, C. Providência, S. Schramm, Astron. Astrophys. **627**, A61 (2019)
[6] T. Inoue (HAL QCD), JPS Conf. Proc. **26**, 023018 (2019), AIP Conf. Proc. **2130**, 020002 (2019)
[7] T. Klähn, T. Fischer, Astrophys. J. **810**, 134 (2015)
[8] M. Cierniak, T. Klähn, T. Fischer, N. Bastian, Univ. **4**, 30 (2018)
[9] I.A. Rather, U. Rahaman, V. Dexheimer, A.A. Usmani, S.K. Patra, Astrophys. J. **917**, 46 (2021)
[10] I.A. Rather, A.A. Usmani, S.K. Patra, Jour. Phys. G: Nucl. and Part. Phys. **48**, 085201 (2021)
[11] E. Farhi, R.L. Jaffe, Phys. Rev. D **30**, 2379 (1984)
[12] W. Wei, B. Irving, M. Salinas, T. Klähn, P. Jaikumar, Astrophys. J. **887**, 151 (2019)
[13] N.K. Glendenning, Phys. Rev. D **46**, 1274 (1992)
[14] V. Dexheimer, B. Franzon, R. Gomes, R. Farias, S. Avancini, S. Schramm, Phys. Lett. B **773**, 487 (2017)
[15] I.A. Rather, A.A. Rather, I. Lopes, V. Dexheimer, A. Usmani, S. Patra, Astrophys. J. **943**, 52 (2023)
[16] D. Chatterjee, T. Elghozi, J. Novak, M. Oertel, MNRAS **447**, 3785 (2015)
[17] LORENE, *Langage objet pour la relativité numérique*, http://www.lorene.obspm.fr (-)
[18] R. Abbott, T.D. Abbott et al., Astrophys. J. **896**, L44 (2020)
[19] P.B. Demorest, T. Pennucci, S.M. Ransom, M.S.E. Roberts, J.W.T. Hessels, Nature **467**, 1081 (2010)
[20] H.T. Cromartie, E. Fonseca *et al.*, Nature Astron. **4**, 72 (2019)
[21] M.C. Miller *et al.*, Astrophys. J. **887**, L24 (2019), Astrophys. J. Lett. **918**, L28 (2021)
[22] T.E. Riley *et al.*, Astrophys. J. **887**, L21 (2019), Astrophys. J. Lett. **918**, L27 (2021)
[23] G. Raaijmakers et al., Astrophys. J. **887**, L22 (2019)